



North Atlantic forcing of millennial-scale Indo-Australian monsoon dynamics during the Last Glacial period



Rhawn F. Denniston^{a,*}, Karl-Heinz Wyrwoll^b, Yemane Asmerom^c, Victor J. Polyak^c, William F. Humphreys^{d,e}, John Cugley^f, David Woods^g, Zachary LaPointe^c, Julian Peota^a, Elizabeth Greaves^a

^a Department of Geology, Cornell College, Mount Vernon, Iowa, USA

^b School of Earth and Environment, University of Western Australia, Perth, Western Australia, Australia

^c Department of Earth and Planetary Sciences, University of New Mexico, Albuquerque, New Mexico, USA

^d School of Animal Biology, University of Western Australia, Perth, Western Australia, Australia

^e Western Australia Museum, Perth, Western Australia, Australia

^f Illawarra Speleological Society, Perth, Western Australia, Australia

^g Department of Environment and Conservation, Broome, Western Australia, Australia

ARTICLE INFO

Article history:

Received 31 January 2013

Received in revised form

18 April 2013

Accepted 19 April 2013

Available online

Keywords:

Stalagmite

Oxygen isotope

Indo-Australian summer monsoon

Kimberley

Last Glacial Maximum

ABSTRACT

Recent studies of the Last Glacial period Indo-Australian summer monsoon (IASM) have revealed links to both northern and southern hemisphere high latitude climate as well as to regional ocean conditions. Particular interest has been paid to the monsoon response to Heinrich events, with variability explained by meridional shifts in positioning of the intertropical convergence zone (ITCZ), but this model has not been adequately tested. In addition, the shorter-lived Dansgaard/Oeschger (D/O) events have not been detected (beyond D/O-1, the Bølling/Allerød) in land-based records from the Indo-Pacific, despite their prominent expression in stalagmites from southern Asia, raising questions about the sensitivity of the IASM to these events. Here we present a Southern Hemisphere stalagmite oxygen isotopic time series from Ball Gown Cave (BGC), tropical northern Australia, located on the margins of the modern austral summer ITCZ, that spans 40–31 and 27–8 ka. Elevated IASM rainfall coincides with Heinrich stadials and the Younger Dryas, while decreased rainfall characterizes D/O interstadials, a response that is anti-phased with sites spanning the Indo-Pacific Warm Pool and with Chinese records of the East Asian summer monsoon. The BGC time series thus reveals a precipitation dipole consistent with a southward (northward) migration of the ITCZ during periods of high northern latitude cooling (warming) as the primary driver of millennial-scale IASM variability during the Last Glacial period. Our record indicates a strengthening of the IASM after the Younger Dryas period, likely as a result of rising sea level and sea surface temperatures, breaking the link with the high latitudes.

© 2013 Elsevier Ltd. All rights reserved.

1. Introduction

Over the Last Glacial cycle, monsoons across Africa (Schefuß et al., 2011; Stager et al., 2011), Asia (Wang et al., 2001; Fleitmann et al., 2003), North America (Asmerom et al., 2010) and South America (Cruz et al., 2005; Wang et al., 2007; Kanner et al., 2012) varied with insolation over orbital time scales, but also exhibited millennial-scale oscillations tied to high latitude climate. Most notably, the Younger Dryas (YD) and Heinrich stadials, periods of high northern latitude cooling recorded in Greenland ice (NGRIP

members, 2004) and marine sediments (Bond et al., 1997), were marked by substantial rainfall anomalies in the Northern (Wang et al., 2001) and Southern (Schefuß et al., 2011) Hemispheres. The impact of these events on rainfall in the (sub)tropics is increasingly well resolved, and is explained, in part, by meridional displacement of the ITCZ due to an expansion of ice cover or decrease in temperature at high northern latitudes, or a reduction in Atlantic Meridional Overturning Circulation, all of which occurred during the YD and Heinrich stadials (Chiang and Bitz, 2005; Lewis et al., 2010).

The ITCZ and the planetary monsoon are closely coupled, particularly in the western Pacific and across the maritime continent, areas that lack prominent topographic features such as the Tibetan Plateau that drive intense atmospheric convection

* Corresponding author.

E-mail address: RDenniston@CornellCollege.edu (R.F. Denniston).

(Suppiah, 1992). As a result, the IASM, which dominates the climate across northern Australia and the Indo-Pacific, is closely linked with sea surface conditions of the Indo-Pacific Warm Pool (IPWP) and has had a somewhat complex evolution through the Last Glacial period. Paleomonsoon reconstructions along a latitudinal transect from eastern Asia through the IPWP reveal significant regional variations. In the Northern Hemisphere, stalagmites from Hulu Cave, China (32°N) (Wang et al., 2001), preserve a Last Glacial record of East Asian summer monsoon (EASM) rainfall that is nearly identical in timing and structure to temperature variations reconstructed from Greenland ice but with clearly defined Heinrich stadials preserved as periods of a weakened EASM, while D/O interstadials were characterized by sharp increases in the EASM (Fig. 1). Stalagmites from Borneo (4°N) (Partin et al., 2007) also suggest a weakened IASM during Heinrich stadial 1 (HS1) (17–15 ka) but they do not record D/O events and instead exhibit a connection to IPWP sea surface temperature (SST) as well as to southern high latitude climate, with decreased IASM rainfall coincident with the Antarctic Cold Reversal (14.5–12.5 ka) (Blunier and Brook, 2001). In the Southern Hemisphere, a stalagmite time series from Flores (8°S) is closely tied to IPWP conditions and also indicates a strengthened IASM during the YD (Griffiths et al., 2009), but the IASM response to Heinrich events at this site is less well constrained (Lewis et al., 2010, 2011). A high-resolution marine

core from the south Java margin (Mohtadi et al., 2011) located at a similar latitude to Flores reveals pronounced millennial-scale changes in terrigenous sedimentation and foraminiferal isotopic chemistry interpreted as a *weakened* IASM during the YD and HS1 (and a strengthened IASM during D/O event 1) while Muller et al. (2012) document *increases* in continental weathering during HS1 from the Flores Sea. Neither the Flores nor the Java record preserves evidence of forcing in response to Antarctic climate, and no continental records from the IPWP record D/O events (other than D/O-1, the Bølling/Allerød). Fully understanding the nature of the IASM response to extra-tropical forcing requires the development of continuous, high-resolution records from the southernmost margin of the IASM. To do so, six cylindrical, calcite stalagmites (BGC5, 6, 10, 11, 14, and 16) (Fig. 2) were collected from BGC (17°2'S, 125°0'E, ~100 m elevation), located in the western Kimberley of tropical Western Australia (Fig. 1). Oxygen isotopic ratios of these samples track monsoon variability, allowing a unique examination of IASM dynamics during the Last Glacial period.

2. Materials and methods

2.1. ^{230}Th dating

Stalagmites were sectioned using a water-cooled saw along the vertical growth axis and inspected for signs of recrystallization. Stalagmite chronologies were constructed using 36 ^{230}Th dates obtained with a Thermo Neptune multi-collector ICP-MS at the University of New Mexico Radiogenic Isotope Laboratory using methods described by Asmerom et al. (2006) (Table 1). For dating, 50–150 mg of calcite was milled at each interval of interest using a computer-guided drill from each interval of interest and then dissolved and spiked with a mixed ^{229}Th – ^{233}U – ^{236}U tracer. The sample and spike were homogenized by drying the solution on a hot plate and then redissolving in 7 N HNO_3 . Any organics included within the calcite were destroyed by heating in 14 N HNO_3 and perchloric acid,

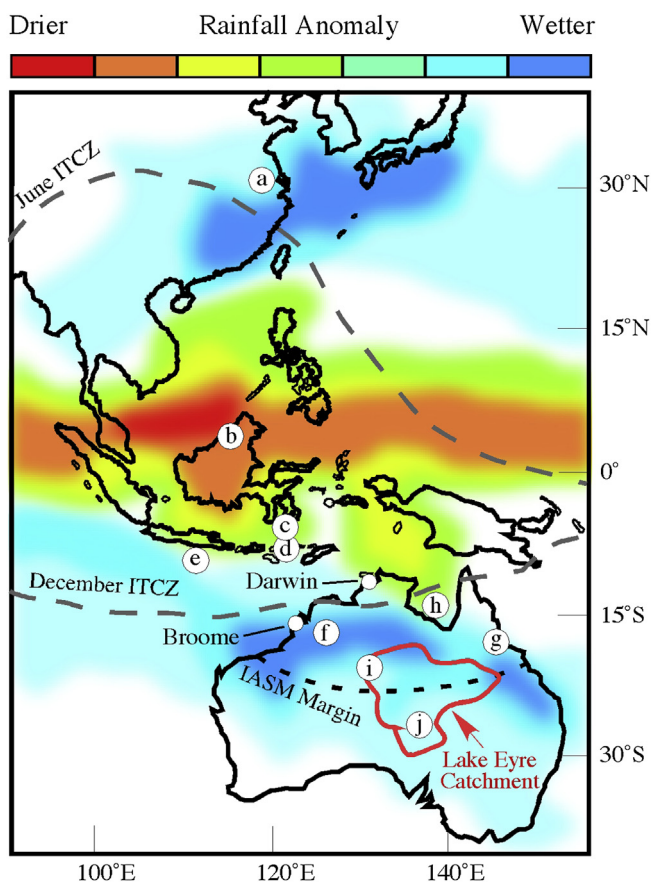


Fig. 1. Map of the western Pacific showing sites discussed in text with DJF rainfall anomalies associated with North Atlantic hosing simulations of Heinrich events (after Lewis et al., 2010): (a) Hulu Cave, China (Wang et al., 2001); (b) Gunung Buda Cave, Borneo (Partin et al., 2007); (c) Flores Sea core VM33-80 (Muller et al., 2012); (d) Liang Luar Cave, Flores (Griffiths et al., 2009); (e) south Java core GeoB 10053-7 (Mohtadi et al., 2011); (f) Ball Gown Cave (this study) and approximate location of Lake Gregory (Wyrwoll and Miller, 2001); (g) Lynch's Crater (Muller et al., 2008); (h) Gulf of Carpentaria (De Deckker, 2001; Reeves et al., 2008); (i) Lake Lewis basin (English et al., 2001); (j) Lake Eyre (Magee et al., 2004).

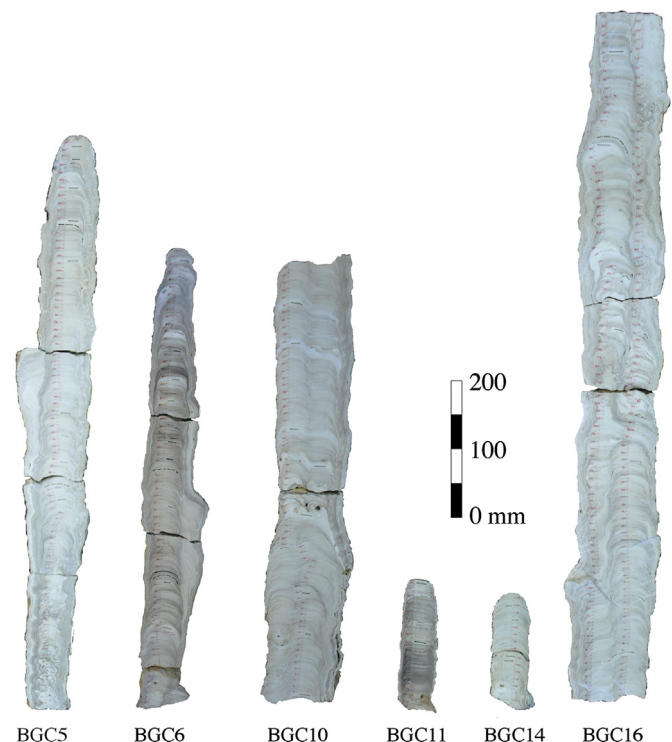


Fig. 2. Cross-section of BGC stalagmites analyzed in this study.

Table 1
U–Th isotopic ratios and ^{230}Th ages.

Sample	mm to bottom	^{238}U (ng/g)	^{232}Th (pg/g)	$\delta^{234}\text{U}$ (meas'd)	Error	$^{230}\text{Th}/^{238}\text{U}$ (activity)	Error	$^{230}\text{Th}/^{232}\text{Th}$ (activity)	Error	Uncorrected age (Yr BP)	Error (Yr)	Corrected age (Yr BP)	Error (Yr)
5	769	31.5	2427	339.1	2.3	0.2972	0.004	11.78	0.259	27,690	400	26,000	1730
5	727	24.2	2901	349.6	3.0	0.3036	0.004	7.75	0.130	28,110	440	25,500	2650
5	463	31.0	581	345.5	1.6	0.2807	0.003	45.72	2.444	25,820	290	25,420	500
5	435	29.3	886	359.2	1.9	0.2923	0.004	29.56	1.641	26,730	450	26,090	790
5	361	29.5	2916	367.8	3.7	0.3036	0.003	9.38	0.158	27,690	360	25,570	2150
5	297	23.7	999	359.5	2.2	0.3057	0.005	22.16	0.928	28,130	510	27,230	1040
6	674	41.2	3064	356.5	2.4	0.0975	0.004	4.01	0.181	8160	340	6550	1640
6	664	45.5	5129	364.1	3.0	0.1029	0.003	2.71	0.079	8575	250	6070	2510
6	649	51.6	5081	350.2	2.5	0.1107	0.001	3.44	0.045	9364	120	7220	2140
6	565	134.5	7996	367.1	1.9	0.1303	0.001	6.70	0.046	10,980	70	9710	1270
6	526	33.1	1467	363.2	1.9	0.1391	0.003	9.57	0.316	11,800	270	10,850	990
6	496	41.0	1667	374.5	1.9	0.1422	0.004	10.68	0.475	11,980	330	11,110	920
6	484	56.3	5341	372.1	2.8	0.1509	0.004	4.86	0.134	12,770	320	10,740	2050
6	472	90.3	1523	373.7	1.5	0.1396	0.002	25.28	1.265	11,750	190	11,390	410
6	463	54.2	7104	371.3	3.4	0.1634	0.003	3.81	0.076	13,900	270	11,090	2830
6	423	143.2	16,113	367.5	2.9	0.1655	0.001	4.49	0.034	14,140	110	11,720	2420
6	356	33.4	2564	372.6	2.7	0.1641	0.004	6.54	0.227	13,970	400	12,330	1680
6	255					Isochron-	see	below				15,100	1500
6	255 iso 1	278.0	264,209	377.1	4.0	0.3286	0.001	1.06	0.004	29,750	140	15,200	3480
6	255 iso 2	166.3	129,450	357.5	5.7	0.2888	0.001	1.13	0.005	26,140	140	15,020	5430
6	255 iso 3	156.5	46,373	370.0	3.4	0.2233	0.001	2.30	0.015	19,460	140	13,590	2900
6	255 iso 4	155.1	31,517	378.1	1.6	0.2105	0.002	3.16	0.027	18,200	160	17,760	270
6	255 iso 5	171.3	66,900	374.3	1.6	0.2314	0.001	1.81	0.011	20,260	130	19,410	440
6	33	26.2	1115	376.1	3.1	0.2035	0.005	14.62	0.636	17,590	430	16,690	1000
10	602	39.5	492	390.2	3.1	0.3902	0.003	95.72	7.546	36,610	340	36,350	430
10	546	40.3	120	384.1	1.5	0.4026	0.002	412.12	89.393	38,230	280	38,170	290
10	431	50.6	219	388.9	1.5	0.4123	0.002	291.58	26.174	39,200	210	39,110	230
10	315	69.9	1756	393.6	1.6	0.4135	0.001	50.30	0.677	39,170	160	38,640	550
11	151	50.7	4113	431.7	2.8	0.1478	0.005	5.57	0.228	11,940	440	10,290	1720
11	113	73.9	7052	452.3	2.9	0.1452	0.002	4.65	0.074	11,550	170	9620	1930
11	91	70.7	2623	466.7	1.8	0.1376	0.001	11.33	0.133	10,810	80	10,070	740
14	139	32.8	4011	630.6	5.2	0.2825	0.004	7.07	0.125	20,990	330	18,790	2220
14	89	21.1	799	554.9	3.5	0.2937	0.012	23.73	3.086	23,150	1030	22,440	1260
14	72	30.5	937	597.2	2.1	0.2932	0.004	29.19	1.308	22,430	310	21,870	640
14	63	22.2	1102	559.0	3.6	0.2836	0.004	17.49	0.574	22,190	350	21,260	990
14	8	35.9	1536	549.4	3.4	0.3092	0.007	22.11	1.356	24,630	590	23,820	1000
16	819	37.0	1267	387.6	2.3	0.3554	0.003	31.68	0.912	32,790	320	32,070	790
16	506	42.4	2180	390.6	2.0	0.4023	0.005	23.90	0.592	37,960	570	36,870	1220
16	187	40.0	456	387.2	1.6	0.3952	0.004	105.96	9.124	37,280	420	37,040	480
16	724	40.4	390	380.1	1.9	0.3584	0.003	113.37	10.872	33,350	290	33,140	360
16	339	69.7	2338	386.6	1.7	0.3771	0.001	34.38	0.396	35,230	150	34,520	720

and the sample was then processed using standard column chemistry methods. For analysis, the U and Th fractions were dissolved in a 3% HNO_3 4 ml solution which was then aspirated into the instrument using a Cetac Aridus II low flow (50–100 $\mu\text{l}/\text{min}$) desolvating nebulizer system. U and Th separates were run as static routines where all isotopes were measured in faraday cups, with the exception of ^{234}U and ^{230}Th , which were measured using the secondary electron multiplier (SEM). Gains between the SEM and the faraday cups were determined using standard solutions of NBL-112 for U and an in-house ^{230}Th - ^{229}Th standard for Th which were measured after approximately every fifth sample; U and Th blanks are <20 pg. Decay constants used are those reported by Cheng et al. (2000). Isochron data were processed using IsoPlot (Ludwig, 1999).

Developing growth models for BGC stalagmites was complicated by their low U concentrations, as well as occasionally high abundances of detrital Th (^{232}Th) and associated unsupported ^{230}Th . In order to constrain the initial $^{230}\text{Th}/^{232}\text{Th}$ ratio, we attempted two separate six sub-sample $^{230}\text{Th}/^{238}\text{U}$ - $^{232}\text{Th}/^{238}\text{U}$ isochrons from each of stalagmites BGC5, BGC-6, and BGC-16, with only one successful outcome and which yielded an initial $^{230}\text{Th}/^{232}\text{Th}$ atomic ratio of 2.4 ± 0.4 ppm (Fig. 3). The reason for the failure of the other isochrons to yield a statistically significant regression is unclear. Because we were unable to develop a coherent isochron-based correction for unsupported ^{230}Th , we applied an initial $^{230}\text{Th}/^{232}\text{Th}$ atomic ratio of 4.4 ppm, the average

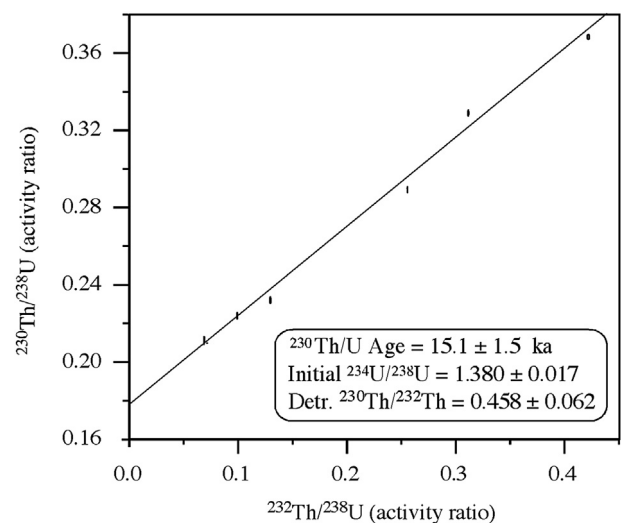


Fig. 3. $^{232}\text{Th}/^{238}\text{U}$ - $^{230}\text{Th}/^{238}\text{U}$ - $^{234}\text{U}/^{238}\text{U}$ three dimensional isochron obtained from stalagmite BGC5. Isochron calculated using IsoPlot (Ludwig, 1999). Values are presented as activity ratios.

crustal silicate value, with an uncertainty of ± 4.4 ppm, to all dates. This value is consistent (within the uncertainty) with that derived from the one successful isochron, and represents a conservative handling of our data. Such an approach increases the reliability of our dates but also results in large age uncertainties, an obstacle we addressed through a high density of samples where possible.

2.2. Stable isotopic analysis

A total of 446 powders were sampled for stable isotopic analysis at regular intervals (varying among stalagmites and dependent on growth rate) from the central growth axis of each stalagmite using a hand-held drill with a 0.5 mm diameter bit. Carbon and oxygen isotopic ratios were measured using a Finnigan MAT 253 coupled with an automated carbonate preparation device (a Kiel III) at the University of Michigan Department of Geological Sciences. All oxygen and carbon isotopic values are presented in parts per mil (‰) relative to the Vienna PeeDee Belemnite carbonate standard (VPDB). The precision of these analyses was monitored with the regular analysis of standards interspersed with the BGC samples and is better than 0.1‰ for both carbon and oxygen isotopic ratios.

3. Environmental setting

3.1. BGC geology

Ball Gown Cave is located in the Napier Range, a massively bedded Devonian reef complex forming an east-west escarpment in the vicinity of Windjana Gorge National Park, 300 km east of Broome, Western Australia. Ball Gown Cave is approximately 500 m long and is characterized by passages that contain numerous restrictions and changes in elevation, all of which serve to reduce air circulation. The stalagmites were collected approximately 300 m from the lower entrance in a single large and well-decorated room. No drips were observed when visited in June 2011, approximately two months after cessation of the monsoon season suggesting that infiltration through the epikarst is rapid and thus little mixing of infiltrated fluids would be expected. Soils over the cave are thin, with exposed karstic limestone prominently exposed.

3.2. IASM rainfall in the western Kimberley

The IASM dominates the climate of the western Kimberley but is a relatively weak system, with sensible heating only observed below 750 hPa (Hung and Yanai, 2004). Primary drivers of monsoon activity are land-sea thermal contrasts, barotropic instability, the Madden-Julien Oscillation, and inflow from the East Asian Winter Monsoon (Wyrwoll and Miller, 2001; Zhang and Zhang, 2010). In the western Kimberley, average summer rainfall exceeds 600 mm and represents ~90% of the yearly total, and annual rainfall decreases sharply with distance south of BGC (Suppiah, 1992) making this site particularly sensitive to IASM variability (Fig. 4).

Seasonal rainfall $\delta^{18}\text{O}$ values at Darwin, Northern Territory, 900 km northeast of BGC but within the same climatic regime, are controlled primarily by amount effects of approximately -1% $100 \text{ mm}^{-1} \text{ month}^{-1}$ ($R^2 = 0.6$; $n > 400$) and no statistically significant correlation with air temperature ($R^2 = 0.06$; $n > 400$) (IAEA/WMO). Although climate modeling reveals the possible role of changing moisture source controls on rainwater $\delta^{18}\text{O}$ values in some portions of the Indo-Pacific during Heinrich events (Lewis et al., 2010; Pausata et al., 2011), the proximity of BGC to the coast, where modern relationships demonstrate the most prominent amount effects to occur (Rozanski et al., 1993), suggests that they would have remained the prominent influence on rainwater

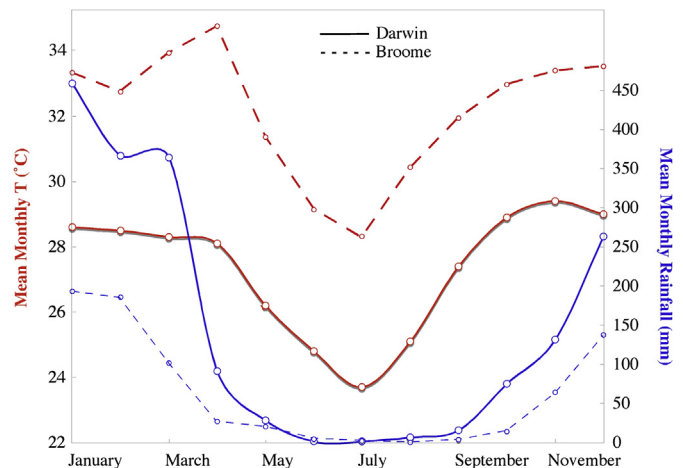


Fig. 4. Climates of Broome, Western Australia (300 km west of BGC) and Darwin, Northern Territory (900 km northeast of BGC) (Australian Bureau of Meteorology, www.BOM.gov.au).

oxygen isotopic ratios during the Last Glacial period. In addition, the temperature dependence of oxygen isotopic fractionation in calcite is small (-0.2% $^{\circ}\text{C}$) (Friedman and O'Neil, 1977) relative to amount effects and thus did not exert a significant influence over BGC stalagmite $\delta^{18}\text{O}$ values.

4. Results

4.1. Stalagmite age models

The low U concentrations (and resulting low supported ^{230}Th abundances) of BGC calcite, as well as uncertainties in the initial $^{230}\text{Th}/^{232}\text{Th}$ ratio, resulted in two standard deviation errors on the ^{230}Th dates averaging $\pm 8\%$. In a small number of cases, particularly high ^{232}Th abundances yielded ages with unacceptably large errors and these results were discarded. Additionally, in one stalagmite, BGC-10, we were unable to obtain any useable dates from the bottom (oldest) 200 mm, and thus we do not present stable isotope data from this section. Including the error window, only a small number of ages fall out of stratigraphic order and reveal stalagmite growth from 40–31 and 27–8 ka (Fig. 5).

Three dates with acceptably small error windows did not fall within error of the growth model for their respective stalagmites (BGC-6 and BGC-16). Two possible explanations for this result, aside from undetected human error during chemical separation or isotopic analysis, are relevant to this discussion. First, although each stalagmite was inspected visually, some speleothem calcite may have experienced alteration or recrystallization that escaped detection. Second, some areas may be characterized by initial $^{230}\text{Th}/^{232}\text{Th}$ ratios outside of the prescribed range (4.4 ± 4.4 ppm). Higher than modeled Th values could explain anomalously young dates, but absent independent techniques for constraining unsupported ^{230}Th (such as isochrons), this question remains unanswered. Where a high density of dates yields internally consistent ages, the age models should be considered robust, but all BGC age models must be viewed in this context.

4.2. Tests for isotopic equilibrium crystallization

A variety of mechanisms, not all of which are related to climate, can influence the oxygen isotopic ratios of speleothem carbonate (Fairchild et al., 2006; Lachniet, 2009). Mickler et al. (2004) studied

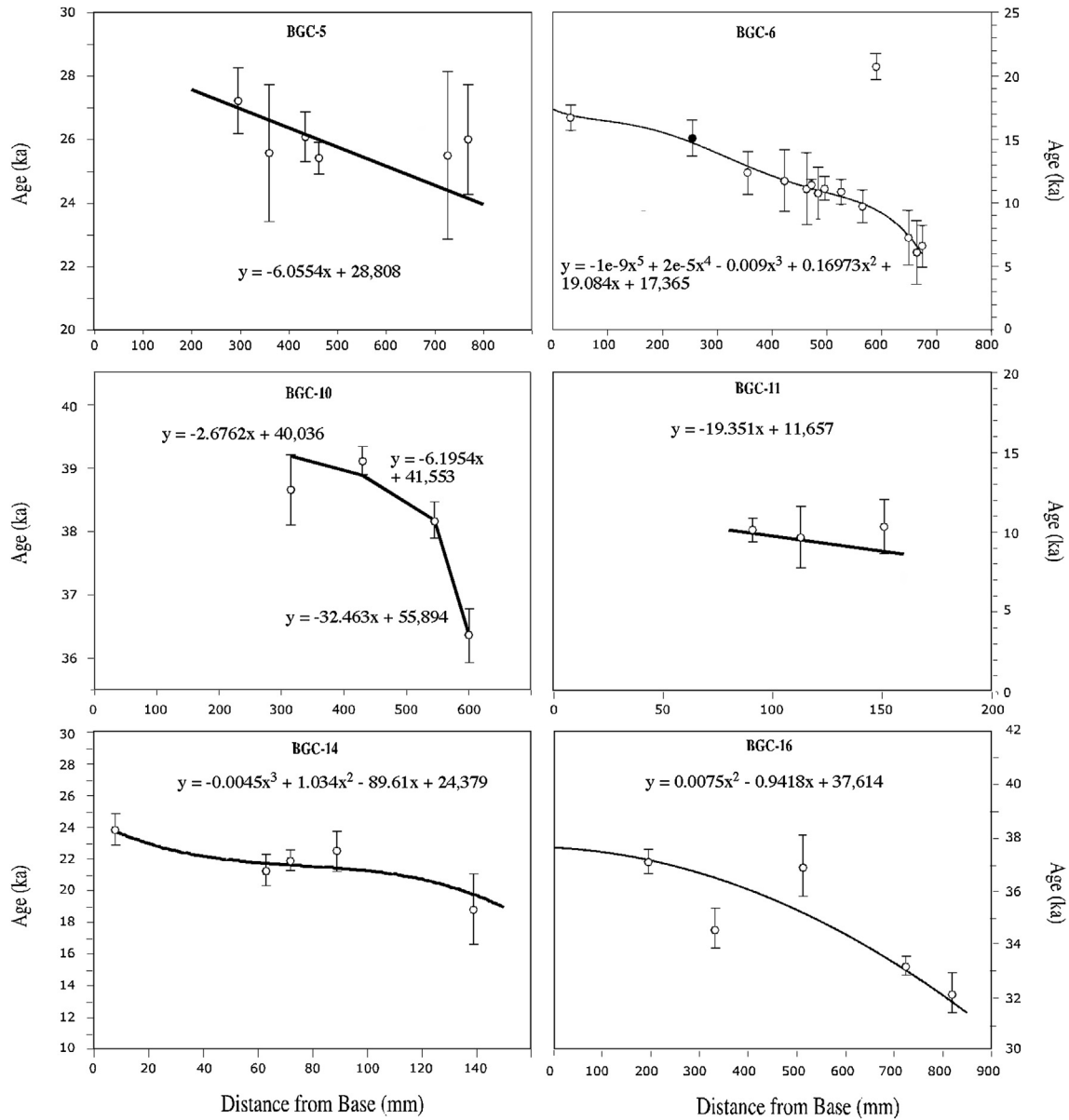


Fig. 5. Age models for BGC stalagmites analyzed in this study. Open circles represent ²³⁰Th ages; closed circle is result of isochron. Vertical lines are two standard deviation errors.

dripwater and cave calcite pairs in modern and fossil stalagmites from a tropical setting and identified oxygen isotopic values both higher and lower than equilibrium values. These authors ascribed their results to a variety of evaporative and kinetic fractionation steps capable of occurring between the soil and the stalagmite growth surface. Because neither cave dripwater nor actively forming stalagmite calcite was identified in BGC, it is not possible to test for equilibrium deposition in the modern setting. Instead, we utilized two methods to assess the degree of equilibrium crystallization of BGC stalagmite calcite. First, we examined the relationship between carbon and oxygen isotopic ratios of each stalagmite. Because the same effects that distort oxygen isotopic ratios can also similarly impact carbon isotopic values, disequilibrium can be suggested by strong covariance of $\delta^{18}O$ and $\delta^{13}C$ values. A wide range in the degree of covariance of BGC stalagmites is apparent, with R^2 values ranging from 0.16–0.57 (Fig. 6). It must also be noted, however, that some paleoenvironmental controls can drive a similar response between these two isotopic systems

and thus this does not constitute a definitive test (Dorale and Liu, 2009).

Second and perhaps more reliably, we compared the stable isotopic values and trends of coeval stalagmites (Fig. 7). Because karstic aquifers are spatially heterogeneous (Perrin et al., 2003) and disequilibrium effects may vary depending on infiltration pathway (Mickler et al., 2004), similar isotopic signatures in stalagmites growing at the same time and under the same conditions should reflect isotopic equilibrium. The BGC stalagmites overlap in age at three intervals: 39–36, 24–22, and 11–8 ka. While our ability to perform this analysis is complicated by the limited resolution of the ²³⁰Th dates, the internal, short-term variability of the oxygen isotopic time series, different temporal resolutions at which the different stalagmites were sampled, and the potential for slightly different microclimates within the areas the stalagmites formed, the degree of overlap is largely suggestive of equilibrium crystallization. The interval 23–22 ka is the exception, with diverging $\delta^{18}O$ trends in the youngest portion of the

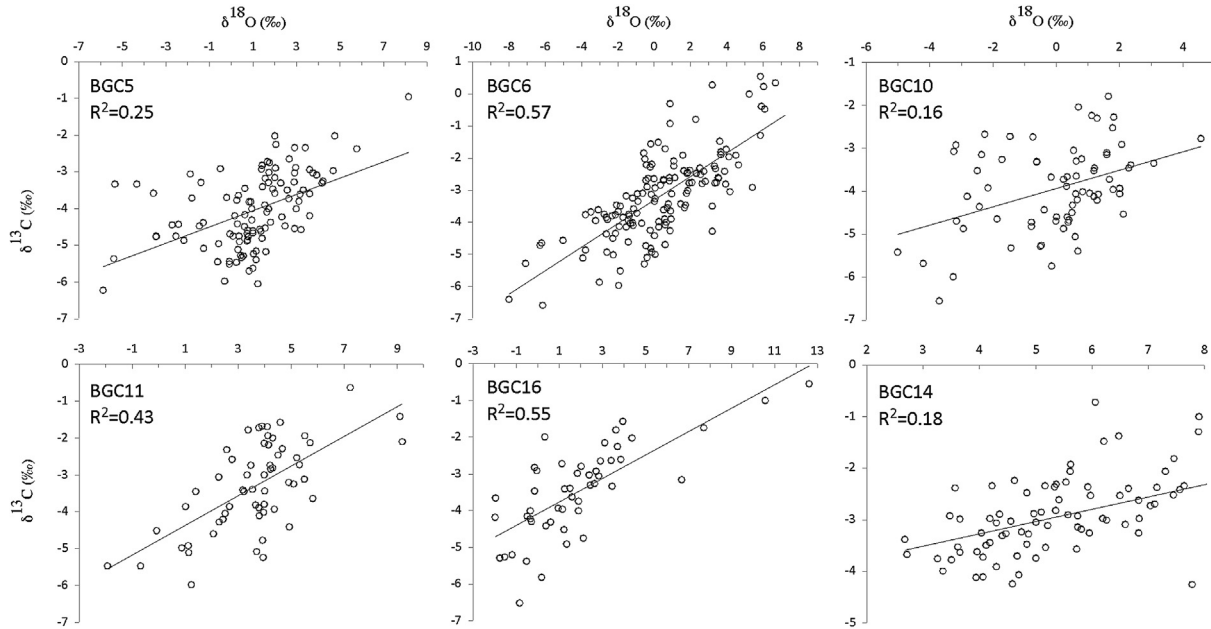


Fig. 6. Analysis of covariance between carbon and oxygen isotopic ratios from BGC stalagmites as a test for isotopic equilibrium crystallization.

overlapping section, but viewing the data in total, we assume that $\delta^{18}\text{O}$ trends in BGC stalagmites track changes in environmental conditions, and primarily amount effects associated with changes in strength of the IASM.

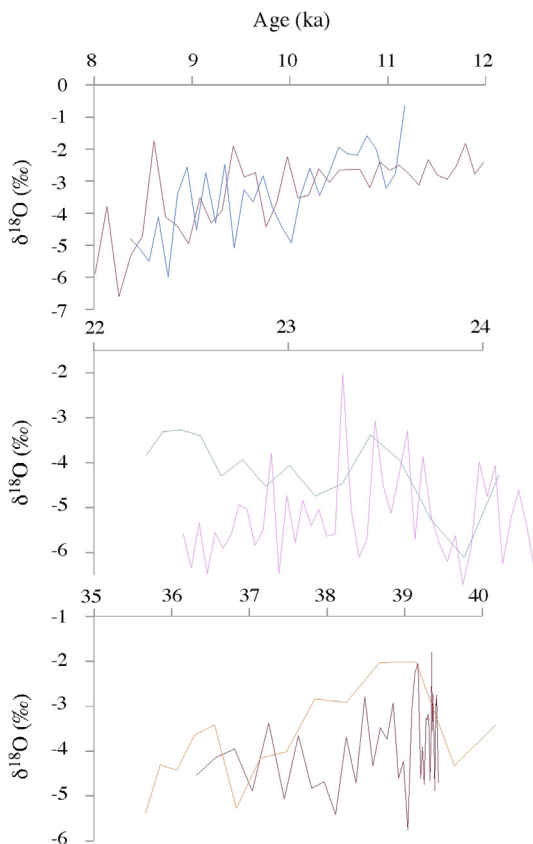


Fig. 7. Oxygen isotopic ratios of coeval BGC stalagmites. Consistent isotopic values and trends in coeval stalagmites suggest isotopic equilibrium crystallization.

5. Discussion

5.1. Last Glacial period IASM variability

The BGC time series reveals a dynamic Last Glacial IASM, including an active albeit variable monsoon occurring across the western Kimberley during the Last Glacial Maximum (LGM) (24–20 ka) (Fig. 8). The general view of this period has been that of a system severely weakened by reduced atmospheric and ocean temperatures, as well as land-sea temperature contrasts (Marshall and Lynch, 2006). This model has evolved, in part, through studies of closed-basin lakes that suggest dry conditions at the LGM. One of the most widely studied proxies for the IASM is the sedimentary record from Lake Eyre, an enormous pluvial lake in south-central Australia that drains a $1.2 \times 10^6 \text{ km}^2$ catchment located largely within the area impacted by the IASM (Fig. 1). Lake Eyre preserves evidence of a fluctuating water table between ~ 40 –12 ka superimposed on overall dry lake conditions (Magee et al., 2004). Lake Eyre itself lies well south of the IASM margin, and as such may not reliably preserve distal and short-term changes in monsoon rainfall, particularly during a period of a generally weakened monsoon. However this explanation does not account for other evidence from pluvial lake and fluvial systems located within the modern IASM regime that support a weakened or collapsed monsoon at the LGM (Bowler et al., 2001).

Punctuating the BGC record are prominent centennial to millennial-scale pulses of rainfall variability with negative isotope anomalies (strengthened monsoon events) coincident with the YD and Heinrich stadials 1 and 2 (Fig. 8). Based on the available chronology, H1 is a broader and more pronounced event than H2, with $\delta^{18}\text{O}$ values decreasing by 3‰ in H1 and 2‰ in H2. Non-uniform responses of the IASM to different H-events has been suggested at sites across IPWP (Partin et al., 2007; Griffiths et al., 2009; Lewis et al., 2011), and may reflect the differential North Atlantic climate anomalies and/or thermohaline circulation changes associated with each H-event. The B/A is marked by a pronounced and sharp weakening of the IASM, and is characterized by the highest $\delta^{18}\text{O}$ values (driest conditions) of the entire BGC

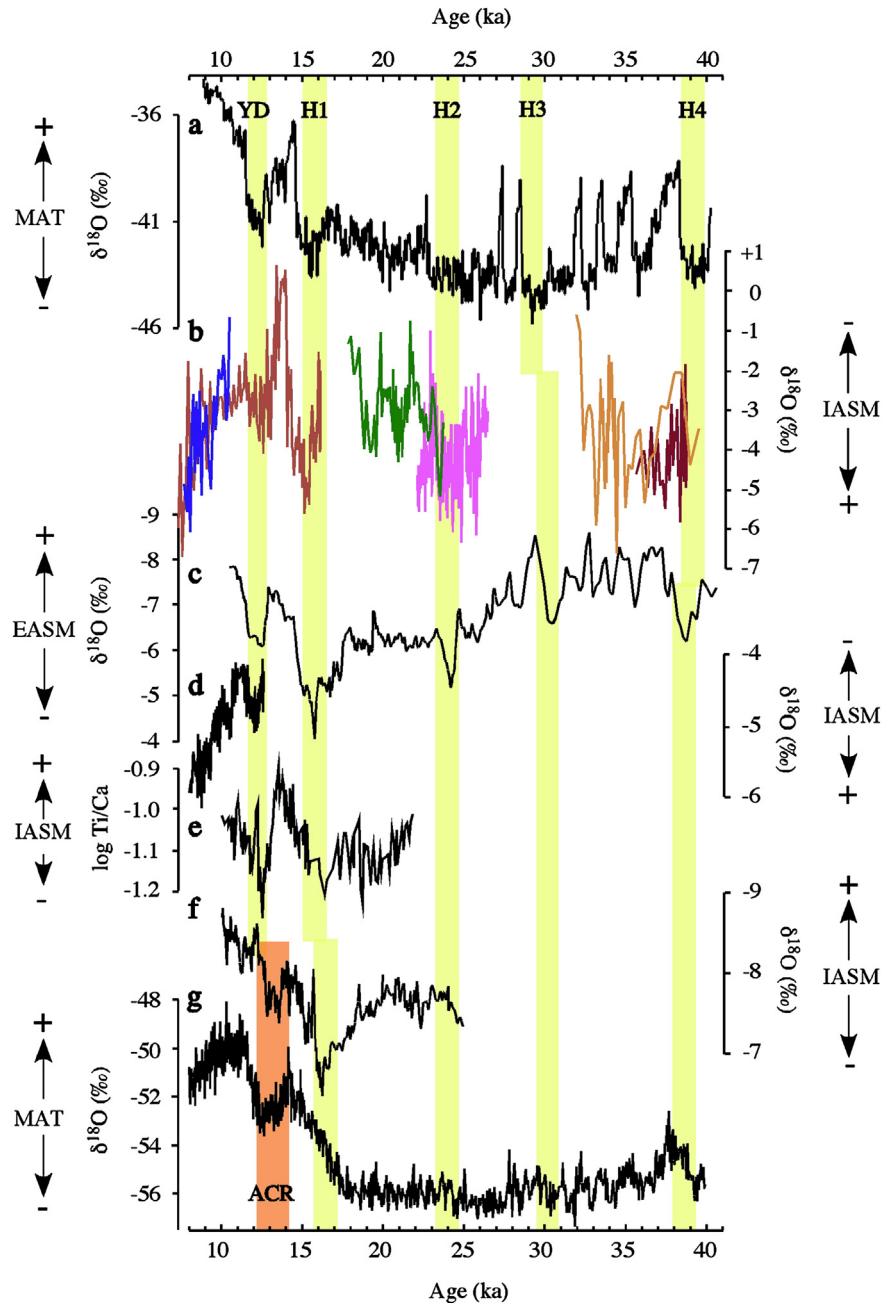


Fig. 8. Records of Last Glacial climate variability. (a) Greenland ice (NGRIP members, 2004); (b) Ball Gown Cave (this study); individual stalgmites are color-coded; (c) Hulu cave, China (Wang et al., 2001); (d) Liang Luar cave, Flores (Griffiths et al., 2009); (e) marine core from south Java (Mohtadi et al., 2011); (f) Gunung Buda cave, Borneo (Partin et al., 2007); (g) EPICA Dome C Antarctica ice core (Stenni et al., 2003). Yellow bars denote Younger Dryas (YD) and Heinrich Stadials (HS) while pink bar denotes Antarctic Cold Reversal (ACR). MAT = mean annual temperature; IASM = Indo-Australian summer monsoon; EASM = East Asian Summer Monsoon.

times series, suggesting that pronounced shifts in hydrologic regime occurred rapidly between 16–13 ka.

The YD (H0) is a considerably less well-defined event than H1. The YD has been identified in continental and marine records from across the IPWP, but its impact on Australia has remained unclear. In fact, based on a review of published studies of deglacial climates, Tibby (2012) argued that no clear expression of the YD is evident anywhere in Australia. The clear expression of the YD in the BGC time series is therefore somewhat surprising and raises the possibility that the influence of the YD would have also been translated across the portion of the Australian interior impacted by the IASM (Fig. 8).

In assessing these findings within the context of earlier regional IASM studies, it is therefore possible that one explanation for the

discrepancies between the BGC time series and nearby fluvial and lake sedimentological studies may lie in the continuity of the different records and the nature of the respective chronological controls. For example, Wyrwoll and Miller (2001) investigated lake levels at Lake Gregory and discharge events at the Fitzroy River, both of which are proximal to Ball Gown Cave and the latter of which is located within the same drainage basin as BGC. These paleo-precipitation studies indicate a sudden change in moisture regime tied to the onset of the monsoon no earlier than 14 ka. While the errors in the BGC chronology limit its temporal resolution to some degree, these stalgmite records strongly suggest that the IASM strengthened, weakened dramatically, and then strengthened

again in association with the H1 - B/A - YD transitions between 16–13 ka. In contrast, the majority of the calibrated radiocarbon ages from Fitzroy River and Lake Gregory fall within one standard deviation error of either the YD or H1. Geomorphic studies identifying pluvial periods at 14 ka may therefore be linked to separate, discrete events not identifiable given the nature of the sedimentological deposits and the chronological resolution available. Supporting this hypothesis is other evidence for dramatic increases in rainfall during the LGM from other areas across tropical Australia. For example, Nott and Price (1994) interpreted an expansion in sediments deposited in plunge pools in the IASM-dominated Northern Territory near Darwin as suggesting pluvial periods between 22–18 ka, and English et al. (2001) used OSL dating to constrain the ages of dune building events in the Lake Lewis basin, central Australia, to 23–21 ka and fluvial deposits at multiple intervals, including at 18, 14, and 11 ka (Fig. 1).

In addition to increases in the IASM strength during the YD and Heinrich stadials, the BGC record, within the prescribed chronological uncertainties, also preserves evidence for a weakened monsoon coincident with D/O interstadials 1–2 and 5–8 (Fig. 8). Oxygen isotopic values associated with these events is quite large (2–3‰), commensurate with the $\delta^{18}\text{O}$ anomaly characterizing the B/A. To date, only a small number of studies have identified climatic oscillations in the Southern Hemisphere coincident with D/O events (Wang et al., 2007; Kanner et al., 2012), despite their clear expression in the Chinese stalagmite record (Wang et al., 2001, 2008). The large magnitude of oxygen isotopic variability that marks D/O events in the BGC record identifies D/O interstadials as prominent climatic events in Western Australia during the Last Glacial period. Thus, the BGC time series reveals a close and continuous link between the IASM and high northern latitude climate variability during the Last Glacial.

5.2. Origins of IASM variability

A commonly invoked mechanism used to explain monsoon dynamics during Heinrich and D/O events is extra-tropical forcing of the ITCZ, with colder high northern latitudes displacing the ITCZ band southward (Chiang and Bitz, 2005; Broccoli et al.,

2006). The BGC record is consistent with this model, and is supported by computer simulations of Heinrich stadials that indicate a poleward propagation of the Southern Hemisphere ITCZ, with the locus of IASM rainfall shifted by approximately 5° latitude from its present location (Lewis et al., 2010), although other models produce more ambiguous results (Lu and Dong, 2008; Yu et al., 2009). These results are also consistent with pollen and elemental data extracted from Lynch's Crater, located in the humid subtropics of northeastern Queensland, which although not entirely influenced by IASM rains, is closely tied to migration of the ITCZ (Muller et al., 2008). If correct, then the fact that the $\delta^{18}\text{O}$ minimum which characterizes the YD is small in relation to H1 or H2 may correspond to a less southerly displacement of the ITCZ and a restriction of enhanced YD-age IASM precipitation to the northern margins of the Australian continent and therefore providing an explanation for its apparent absence across the Australian interior.

Additionally, some forcing of millennial-scale events at BGC may be related to cross-equatorial linkages between the EAWM and IASM, particularly with respect to southward outflow associated with the Siberian High during boreal winter (austral summer). Clear examples of EAWM influences on IASM rainfall have been documented from recent regional climatic events, such as the dramatic "cold surges" of 2008 AD that produced deep convective flare-up over northern Australia and Indonesia and a strengthened IASM (Hong and Li, 2009). Anti-phasing of the East Asian summer and winter monsoons has been suggested (Yancheva et al., 2007), and if correct, then the strengthened EASM occurring during D/O interstadials (and between Heinrich stadials) would have coincided with a weakened cross-equatorial flow, diminishing IASM rainfall in the Australian tropics.

The BGC record also allows a reconciliation of seemingly contradictory short-term monsoon dynamics from the Australian tropics, which to date have been reconstructed using proxies that offer limited temporal resolution (Nott and Price, 1994; Wyrwoll and Miller, 2001; van der Kaars and De Deckker, 2002; Magee et al., 2004) and/or a somewhat ambiguous link to the IASM (Cohen et al., 2011). One of the few higher resolution records attributed directly to IASM variability is from the northern Australia

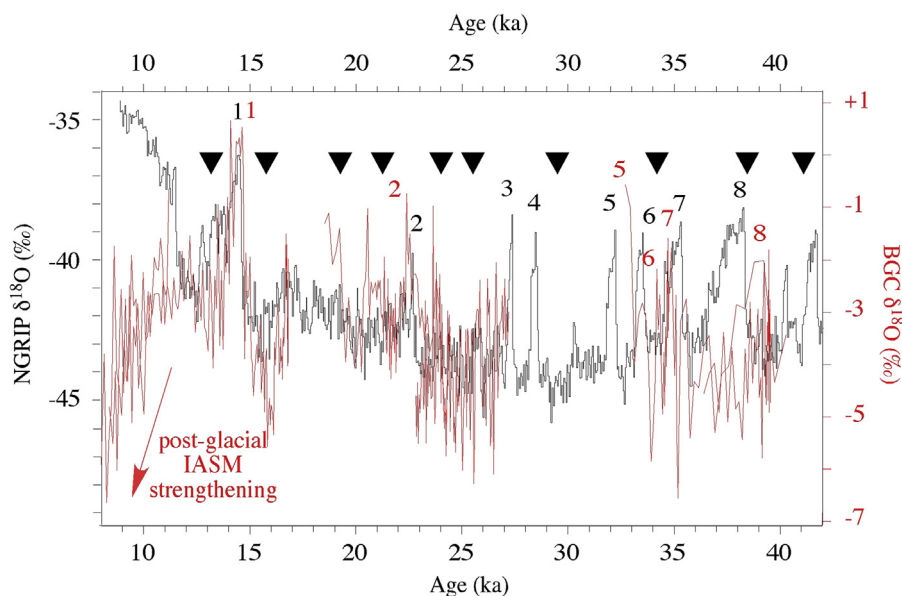


Fig. 9. Comparison of NGRIP ice core (NGRIP members, 2004) (black) and stacked Ball Gown Cave (red) oxygen isotope records. Numbers denote D/O interstadials in the respective time series. Black triangles denote intervals of peak aridity at Lake Carpentaria (De Deckker, 2001; Reeves et al., 2008) that correspond with intervals of strengthened IASM rainfall at BGC. IASM = Indo-Australian summer monsoon. This manuscript benefitted from comments by two anonymous reviewers.

continental shelf in the modern Gulf of Carpentaria (Fig. 1). Here, sediments from a Last Glacial period lake preserve episodes of sand deposition (De Deckker, 2001) that closely match periods of elevated monsoon rainfall in the BGC record (Fig. 9). These sedimentary packages, which are interpreted to represent increases in fluvial discharge (Reeves et al., 2008), or possibly dune mobility (De Deckker, 2001), are coincident with periods of elevated IASM rainfall at BGC, including two isotopic excursions at 24 and 26 ka, events not apparent in either the Greenland or Hulu cave records (Figs. 8 and 9). This observed relationship linking the western Kimberley and the Gulf of Carpentaria argues for the BGC record to be representative of a broad regional response across the Australian tropics during the Last Glacial period.

Because periods of high northern latitude warming (such as marks the end of the YD) are coincident with a weakened monsoon in the western Kimberley during the Last Glacial period, then IASM rainfall would have been expected to decrease sharply after 11.5 ka. Instead of diminishing, however, the IASM gained strength, marking the onset of enhanced early Holocene monsoon conditions, likely in response to changing ocean conditions in the IPWP, including flooding of the Sahul and Sunda continental shelves and rising regional SST, both of which were underway by at least 12 ka (Bard, 1996; Wyrwoll and Miller, 2001; Stott et al., 2002). This response is similar to that recorded in stalagmites from Flores (Griffiths et al., 2009) and appears to reflect a regional-scale monsoon response. The links to the high northern latitudes evident in the BGC record between 40 and 12 ka were broken at the Holocene/Pleistocene transition as regional controls on the IASM became enhanced and ice cover at the high northern latitudes decreased in association with the early phases of deglaciation.

6. Conclusions

When the BGC record is placed in a regional context, the overall picture that emerges is a consistent monsoon response to extra-tropical forcing across the IPWP, with regions located north of the austral summer ITCZ experiencing decreased rainfall during periods of high northern latitude cooling, and regions located south of the austral summer ITCZ (e.g., BGC) experiencing increased monsoon rainfall. H-events (including the YD) are clearly expressed as periods of increased IASM rainfall. While the BGC time series lacks the requisite chronological control to definitively tie millennial-scale oxygen isotopic variability to distal climate events, taken at face value, these data also support a similar relationship between the IASM and D/O events.

The stalagmite record from Borneo remains the anomalous link to IPWP SST and to the southern high latitudes. No evidence in the BGC record links the IASM to Antarctica, but instead emphasizes the role played by the Northern Hemisphere on the Last Glacial evolution of the IASM. At the Holocene/Pleistocene transition, regional ocean conditions, including SST and flooding of continental shelf, broke the link to the extra-tropical forcing at the start of the Holocene, a response consistent with IASM reconstructions from the southern IPWP.

Acknowledgments

We gratefully acknowledge the Kimberley Land Council and the Australian Department of Environment and Conservation for their assistance with this research. Funding for this work was provided by the Kimberley Foundation Australia (to KHW), and the National Science Foundation of the United States (1103413), the Center for Global and Regional Environmental Research, and

Cornell College (to RFD). We thank Donna Cavlovic for assistance in Kununurra.

References

- Asmerom, Y., Polyak, V., Schwieters, J., Bouman, C., 2006. Routine high-precision U–Th isotope analyses for paleoclimate chronology. *Geochimica et Cosmochimica Acta* 70, A24.
- Asmerom, Y., Polyak, V.J., Burns, S.J., 2010. Variable winter moisture in the southwestern United States linked to rapid glacial climate shifts. *Nature Geoscience* 3, 114–117.
- Australian Bureau of Meteorology: www.bom.gov.au (accessed 2010).
- Bard, E., 1996. Deglacial sea-level record from Tahiti corals and the timing of global meltwater discharge. *Nature* 382, 241–244.
- Blunier, T., Brook, E.J., 2001. Timing of millennial-scale climate change in Antarctica and Greenland during the last glacial period. *Science* 291, 109–112.
- Bond, G., Showers, W., Cheseby, M., Lotti, R., Almasi, P., deMenocal, P., Priore, P., Cullen, H., Hajdas, I., Bonani, G., 1997. A pervasive millennial-scale cycle in North Atlantic Holocene and glacial climates. *Science* 278, 1257–1266.
- Bowler, J.M., Wyrwoll, K.-H., Lu, Y., 2001. Variations of the northwest Australian summer monsoon over the last circa 300,000 years: the palaeohydrological record of the Gregory Lakes System. *Quaternary International* 83–85, 63–80.
- Broccoli, J.E., Dahl, K.A., Stouffer, R.J., 2006. Response of the ITCZ to northern hemisphere cooling. *Geophysical Research Letters* 33, L01702.
- Cheng, H., Edwards, R.L., Hoff, J., Gallup, C.D., Richards, D.A., Asmerom, Y., 2000. The half-lives of U-234 and Th-230. *Chemical Geology* 169, 17–33.
- Chiang, J.C.H., Bitz, C.M., 2005. Influence of high latitude ice cover on the marine Intertropical Convergence Zone. *Climate Dynamics*. <http://dx.doi.org/10.1007/s00382-005-0040-5>.
- Cohen, T.J., Nanson, G.C., Jansen, J.D., Jones, B.G., Jacobs, Z., Treble, P., Price, D.M., May, J.-H., Smith, A.M., Ayliffe, L.K., Hellstrom, J.C., 2011. Continental aridification and the vanishing of Australia's megalakes. *Geology* 39, 167–170.
- Cruz, F.W., Burns, S.J., Karmann, I., Sharp, W.D., Vuille, M., Cardoso, A.O., Ferrari, J.A., Silva Dias, P.L., Viana, O., 2005. Insolation-driven changes in atmospheric circulation over the past 116,000 years in subtropical Brazil. *Nature* 434, 63–66. <http://dx.doi.org/10.1038/nature03365>.
- De Deckker, P., 2001. Late Quaternary cyclic aridity in tropical Australia. *Palaeogeography, Palaeoclimatology, Palaeoecology* 170, 1–9.
- Dorale, J.A., Liu, Z., 2009. Limitations of Hendy test criteria in judging the paleoclimatic suitability of speleothems and the need for replication. *Journal of Cave and Karst Studies* 71, 73–80.
- English, P., Spooner, N.A., Chappell, J., Questiaux, D.G., Hill, N.G., 2001. Lake Lewis basin, central Australia: environmental evolution and OSL chronology. *Quaternary International* 83–85, 81–101.
- Fairchild, I.J., Smith, C.L., Baker, A., Fuller, L., Spotl, C., Matthey, D., McDermott, F., E.I.M.F., 2006. Modification and preservation of environmental signals in speleothems. *Earth-Science Reviews* 75, 105–153.
- Fleitmann, D., Burns, S.J., Mudelsee, M., Neff, U., Kramers, J., Mangini, A., Matter, A., 2003. Holocene forcing of the Indian monsoon recorded in a stalagmite from southern Oman. *Science* 300, 1737–1739.
- Friedman, I., O'Neil, J.R., 1977. Compilation of stable isotopic fractionation factors of geochemical interest. In: Fleischer, M. (Ed.), *Data of Geochemistry Chapter KK: U.S. Geological Survey Professional Paper* 440-K.
- Griffiths, M.L., Drysdale, R.N., Gagan, M.K., Zhao, J.X., Ayliffe, L.K., Hellstrom, J.C., Hantoro, W.S., Frisia, S., Feng, Y.X., Cartwright, I., Pierre, E.S., Fischer, M.J., Suwargadi, B.W., 2009. Increasing Australian-Indonesian monsoon rainfall linked to early Holocene sea-level rise. *Nature Geoscience* 2, 636–639. <http://dx.doi.org/10.1038/ngeo605>.
- Hong, C.-C., Li, T., 2009. The extreme cold anomaly over southeast Asia in February 2008: roles of ISO and ENSO. *Journal of Climate* 22, 3787–3801.
- Hung, C.-W., Yanai, M., 2004. Factors contributing to the onset of the Australian summer monsoon. *Quarterly Journal Royal Meteorological Society* 130, 739–758.
- IAEA/WMO: Global Network of Isotopes in Precipitation. The GNIP Database, <http://isohis.iaea.org>.
- Kanner, L.C., Burns, S.J., Cheng, H., Edwards, R.L., 2012. High-latitude forcing of the South American summer monsoon during the Last Glacial. *Science* 335, 570–573.
- Lachniet, M., 2009. Climatic and environmental controls on speleothem oxygen isotope values. *Quaternary Science Reviews* 28, 412–432.
- Lewis, S.C., LeGrande, A.N., Kelley, M., Schmidt, G.A., 2010. Water vapour source impacts on oxygen isotope variability in tropical precipitation during Heinrich events. *Climate of the Past Discussions* 6, 87–133.
- Lewis, S.C., Gagan, M.K., Ayliffe, L.K., Zhao, J.-x., Hantoro, W.S., Treble, P.C., Hellstrom, J.C., LeGrande, A.N., Kelley, M., Schmidt, G.A., Suwargadi, B.W., 2011. High-resolution stalagmite reconstructions of Australian-Indonesian monsoon rainfall variability during Heinrich stadial 3 and Greenland interstadial 4. *Earth and Planetary Science Letters* 303, 133–142.
- Lu, R.Y., Dong, B.-W., 2008. Response of the Asian summer monsoon to weakening of Atlantic thermohaline circulation. *Advances in Atmospheric Sciences* 25, 723–736.

- Ludwig, K.R., 1999. Using Isoplot/Ex, Version 2.01: a Geochronological Toolkit for Microsoft Excel. Berkeley Geochronology Center Special Publication, Berkeley, California. No. 1a, 47.
- Magee, J.W., Miller, G.H., Spooner, N.A., Questiaux, D., 2004. Continuous 150 k.y. monsoon record from Lake Eyre, Australia: insolation-forcing implications and unexpected Holocene failure. *Geology* 32, 885–888.
- Marshall, A.G., Lynch, A.H., 2006. Time-slice analysis of the Australian summer monsoon during the late Quaternary using the Fast Ocean Atmosphere Model. *Journal of Quaternary Science* 21, 789–801.
- Mickler, P.J., Banner, J.L., Stern, L., Asmerom, Y., Edwards, R.L., Ito, E., 2004. Stable isotope variations in modern tropical speleothems: evaluating equilibrium vs. kinetic isotope effects. *Geochimica et Cosmochimica Acta* 68, 4381–4393.
- Mohtadi, M., Oppo, D.W., Steinke, S., Stuut, J.-B.W., de Pol-Holz, R., Hebbeln, D., Luckge, A., 2011. Glacial to Holocene swings of the Australian-Indonesian monsoon. *Nature Geoscience* 4, 540–544. <http://dx.doi.org/10.1038/NGEO1209>.
- Muller, J., Kylander, M., Wust, R.A.J., Weiss, D., Martinez-Cortizas, A., LeGrande, A.N., Jennerjahn, T., Behling, H., Anderson, W.T., Jacobson, G., 2008. Possible evidence for wet Heinrich phases in tropical NE Australia: the Lynch's Crater deposit. *Quaternary Science Reviews* 27, 468–475. <http://dx.doi.org/10.1016/j.quascirev.2007.11.006>.
- Muller, J., McManus, J.F., Oppo, D.W., Francois, R., 2012. Strengthening of the northeast monsoon over the Flores Sea, Indonesia, at the time of Heinrich event 1. *Geology* 40, 635–638.
- North Greenland Ice Core Project members, 2004. High-resolution record of northern hemisphere climate extending into the last interglacial period. *Nature* 431, 147–151.
- Nott, J., Price, D., 1994. Plunge pools and paleoprecipitation. *Geology* 22, 1047–1050.
- Partin, J.W., Cobb, K.M., Adkins, J.F., Clark, B., Fernandez, D.P., 2007. Millennial-scale trends in west Pacific warm pool hydrology since the last glacial maximum. *Nature* 449, 452–455. <http://dx.doi.org/10.1038/nature06164>.
- Pausata, F.S.R., Battisti, D.S., Nisancioglu, K.H., Bitz, C.M., 2011. Chinese stalagmite $\delta^{18}\text{O}$ controlled by changes in the Indian monsoon during a simulated Heinrich event. *Nature Geoscience*. <http://dx.doi.org/10.1038/NGEO1169>.
- Perrin, J., Jeannin, P.Y., Zwahlen, F., 2003. Implications of the spatial variability of infiltration-water chemistry for the investigations of a karst aquifer: a field study at Milandre test site, Swiss Jura. *Hydrogeology Journal* 11, 673–686.
- Reeves, J.M., Chivas, A.R., Garcia, A., Holt, S., Couapel, M.J.J., Jones, B.G., Cendon, D.I., Fink, D., 2008. The sedimentary record of palaeoenvironments and sea-level change in the Gulf of Carpentaria, Australia, through the last glacial cycle. *Quaternary International* 183, 3–22.
- Rozanski, K., Araguas-Araguas, L., Gonfiantini, R., 1993. Isotopic patterns in modern global precipitation. In: Swart, P.K., Lohmann, K.C., McKenzie, J., Savin, S. (Eds.), *Climate Change in Continental Isotopic Records*. Geophysical Monograph, 78. American Geophysical Union, Washington, DC, pp. 1–36.
- Schefuß, E., Kuhlmann, H., Mollenhauer, G., Prange, M., Patzold, J., 2011. Forcing of wet phases in southeast Africa over the past 17,000 years. *Nature* 480, 509–512.
- Stager, J.C., Ryves, D.B., Chase, B.M., Pausata, F.S.R., 2011. Catastrophic drought in the Afro-Asian monsoon region during Heinrich event 1. *Science* 331, 1299–1302.
- Stenni, B., Jouzel, J., Masson-Delmotte, V., Rothlisberger, R., Castellano, E., Cattani, O., Falourd, S., Johnsen, S.J., Longinelli, A., Sachs, J.P., Selmo, E., Souchez, R., Steffensen, J.P., Udisti, R., 2003. A late-glacial high-resolution site and source temperature record derived from the EPICA Dome C isotope records (East Antarctica). *Earth and Planetary Science Letters* 217, 183–195.
- Stott, L., Poulsen, C., Lund, S., Thunell, R., 2002. Super ENSO and global climate oscillations at millennial time scales. *Science* 297, 222–226.
- Suppiah, R., 1992. The Australian summer monsoon: a review. *Progress in Physical Geography* 16, 283–318.
- Tibby, J., 2012. The Younger Dryas: relevant in the Australian region? *Quaternary International* 253, 47–54.
- van der Kaars, S., De Deckker, P., 2002. A Late Quaternary pollen record from deep-sea core Fr10/95, GC17 offshore Cape Range Peninsula, northwestern Australia. *Review of Palaeobotany and Palynology* 120, 17–39.
- Wang, Y.J., Cheng, H., Edwards, R.L., An, Z.S., Wu, J.Y., Shen, C.C., Dorale, J.A., 2001. A high-resolution absolute-dated late Pleistocene monsoon record from Hulu Cave, China. *Science* 294, 2345–2348. <http://dx.doi.org/10.1126/science.1064618>.
- Wang, X., Auler, A.S., Edwards, R.L., Cheng, H., Ito, E., Wang, Y., Kong, X., Solheid, M., 2007. Millennial-scale precipitation changes in southern Brazil over the past 90,000 years. *Geophysical Research Letters* 34, L23701.
- Wang, Y., Cheng, H., Edwards, R.L., Kong, X., Shao, X., Chen, S., Wu, J., Jiang, X., Wang, X., An, Z., 2008. Millennial- and orbital-scale changes in the east Asian monsoon over the past 224,000 years. *Nature* 451, 1090–1093.
- Wyrwoll, K.-H., Miller, G.H., 2001. Initiation of the Australian summer monsoon 14,000 years ago. *Quaternary International* 83–85, 119–128.
- Yancheva, G., Nowaczyk, N.R., Mingram, J., Dulski, P., Schettler, G., Negendank, J.F.W., Liu, J., Sigman, D.M., Peterson, L.C., Haug, G.H., 2007. Influence of the inter-tropical convergence zone on the east Asian Monsoon. *Nature* 445, 74–78.
- Yu, L., Gao, Y., Wang, H., Guo, D., Li, S., 2009. The responses of east Asian summer monsoon to the North Atlantic meridional overturning circulation in an enhanced freshwater input simulation. *Chinese Science Bulletin* 54, 4724–4732.
- Zhang, C., Zhang, H., 2010. Potential impact of east Asian winter monsoon on climate variability and predictability in the Australian summer monsoon region. *Theoretical and Applied Climatology* 101, 161–177. <http://dx.doi.org/10.1007/s00704-009-0246-2>.